Split-operator spectral method for solving the time-dependent Schrödinger equation in spherical coordinates

Mark R. Hermann and J. A. Fleck, Jr.
Lawrence Livermore National Laboratory, Livermore, California 94550
(Received 5 February 1988)

A spectral method previously developed for solving the time-dependent Schrödinger equation in Cartesian coordinates is generalized to spherical polar coordinates. The solution is implemented by repeated application of a unitary evolution operator in symmetrically split form. The wave function is expanded as a Fourier series in the radial coordinate and in terms of Legendre functions in the polar angle. The use of appropriate quadrature sets makes the expansion exact for band-limited functions. The method is appropriate for solving explicitly time-dependent problems, or for determining stationary states by a spectral method. The accuracy of the method is established by computing the Stark shift and lifetime of the 1*s* state in hydrogen, the low-lying energy levels for hydrogen in a uniform magnetic field, and the 2*p*-*nd* dipole transition spectrum for hydrogen.

I. INTRODUCTION

In recent years interest has grown in the direct numerical solution of the time-dependent Schrödinger equation for solving problems involving time-dependent interactions.[1] The use of time-dependent methods allows the system to be described by the dynamics of an always-square-integrable wave packet. Thus problems involving ionization can be studied in the same straightforward manner as problems involving purely bound-state processes. Furthermore, the evolution of a wave packet in time is of interest because of its close analogy with classical trajectories.[2]

In several previous publications[3–5] a spectral method has been described for solving the time-dependent Schrödinger equation in Cartesian coordinates with a split-operator form of the unitary evolution operator and a finite or band-limited Fourier series representation of the time-dependent wave function. The method is applicable at the same time to the time-dependent description of the motion of a wave packet in a potential and to the determination, by correlation and spectral techniques, of the energy levels and corresponding energy eigenfunctions for the stationary states that compose the wave packet. The method has two very important advantages: the unitarity of the evolution operator preserves the norm of the wave function and thus guarantees conservation of probability and unconditional stability of the method, and the band-limited Fourier series form of the solution allows spatial derivatives to be calculated with much greater accuracy than is possible with finite-difference approximations.

The spectral method is both simple and efficient to apply in Cartesian coordinates because of the availability of the fast-Fourier-transform (FFT) algorithm, but Cartesian coordinates are not the most convenient for solving some physical problems. For example, an electron in a Coulomb field perturbed by an external field, either static or time varying, would be more appropriately described in some type or curvilinear coordinates, such as spherical polar coordinates. In this case an appropriate orthogonal expansion set or basis could be the product of spherical harmonics $Y_{lm}(\theta,\phi)$ and the radial functions $\sin k\pi r/R$. One can apply FFT methods to the radial coordinate at least, but nothing of comparable efficiency is available for the angular variables. For some problems, however, it is possible to use a computational grid with a large number of radial divisions but with relatively few angular divisions and, consequently, relatively few terms in the spherical harmonic expansion to manipulate. Thus one could achieve a significant gain in efficiency over a computation in Cartesian coordinates, which would require a large number of grid points in three orthogonal directions.

In this paper we extend the split-operator spectral technique developed in Refs. 3–5 to spherical polar coordinates. The end result is a scheme which parallels its Cartesian counterpart in many ways including the preservation of the unitarity of the evolution operator and the guarantee of high accuracy, provided the solution is known to be band limited in both its radial and angular dependence. The key to the method is the use of an orthogonal angular polynomial set and a related set of quadrature points and weights that permits a unitary transformation between angle space and angular momentum space analogous to the unitary transformation between configuration and momentum space inherent in the FFT. A split-operator scheme, suitable for use in the description of a hydrogen atom in a strong magnetic field, is also derived. This scheme utilizes a band-limited Fourier series in the axial or z direction and Landau functions in the radial direction. Again the key to this scheme is a quadrature set that permits a unitary transformation between the radial quadrature points and the Landau function expansion coefficients.

The resulting schemes are both versatile and accurate and are suitable for solving true time-dependent problems, e.g., the description of the interaction of an atom with a time varying electric field, or for determining eigenstates by correlation and spectral analysis, which is

normally carried out by time-independent techniques such as the variational method. In this paper, the emphasis is on the latter application, since our aim is to establish the accuracy and versatility of the method. Applications of the method to the description of strictly time-dependent phenomena such as multiphoton absorption will be covered in subsequent articles.

In this paper we describe results for three different applications for which results are obtainable by other methods: the Stark shift and lifetime of the $1s$ state of hydrogen, the energy levels of hydrogen in intermediate and strong magnetic fields, and the calculation of oscillator strengths and final state energies for dipole transitions involving high Rydberg states of hydrogen. Agreement between the split-operator spectral-method results and those obtained with the specialized-reference techniques is in general very good, although the efficiency of the spectral method is not necessarily competitive with the method of choice. An advantage of the spectral method, on the other hand, is its versatility. By turning a crank, so to speak, one can apply it to a wide variety of problems with the expectation of very good accuracy. But its most important advantage is that it can be applied with relative ease to a wide range of time-dependent problems that are at best cumbersome and difficult to solve by other methods.

The paper is organized as follows. In Sec. II the split-operator method is adapted to spherical coordinates. The spectral method for determining energy eigenvalues from time-dependent solutions of the Schrödinger equation is reviewed in Sec. III. In Sec. IV the split-operator method in combination with the spectral method is used to calculate the energy shift and lifetime of the $1s$ state of hydrogen in a static electric field. In Sec. V a form of the split-operator method, based on Landau functions, is developed for treating high magnetic fields. Calculations of the energy levels of a hydrogen atom in a uniform magnetic field are presented in Sec. VI, and in Sec. VII final-state energies and dipole oscillator strengths for a set of transitions in field-free hydrogen are calculated from the time dependent evolution of a wave packet.

Future applications of the method will include studies of the dynamics of high Rydberg states in external magnetic fields and microwave fields along with their implications for quantum chaos, the multiple photon ionization of hydrogen by short intense laser pulses, and multiphoton processes involving vibrating and rotating diatomic and polyatomic molecules.

II. DEVELOPMENT OF THE SPLIT-OPERATOR SPECTRAL METHOD FOR SPHERICAL POLAR COORDINATES

In this section the split-operator spectral method is adapted to spherical polar coordinates. While the discussion is directed towards the specific application of a hydrogen atom in an external electric or magnetic field, the results are clearly applicable to any single particle problem that can be described in spherical polar coordinates with axial symmetry.

The time evolution of the physical system is described by the state function $\Psi(t)$, which satisfies Schrödinger's equation of motion

$$i\frac{\partial}{\partial t}\Psi(t)=H\Psi(t)\ . \tag{1}$$

The Hamiltonian for a hydrogen atom in a static external field can be written in atomic units and spherical polar coordinates as

$$H=-\frac{1}{2m}\frac{\partial^2}{\partial r^2}+\frac{L^2}{2mr^2}-\frac{1}{r}+W(r,\theta)\ , \tag{2}$$

where H is meant to operate on the reduced wave function $\Phi=r\Psi$ and L^2 is the total angular momentum operator. The potentials for the interaction of a hydrogen atom with a homogeneous dc electric field (Stark effect) and a magnetic field (Zeeman effect) are, respectively,

$$W^{\text{Stark}}(r,\theta)=-Fr\cos\theta\ , \tag{3a}$$

$$W^{\text{Zeeman}}(r,\theta)=-\frac{1}{2m}\alpha BL_z+\frac{1}{8m}\alpha^2B^2r^2(1-\cos^2\theta)\ , \tag{3b}$$

where F and B are the electric and magnetic field strengths in atomic units and α is the fine structure constant.

A. Split-operator formalism

The formal expression for advancing the wave function one time increment Δt is

$$\Phi(t+\Delta t)=e^{-iH\Delta t}\Phi(t)\ ,$$

which is approximated by the split-operator expression

$$\begin{aligned}\Phi(t+\Delta t)=&e^{(i\Delta t/4m)\partial^2\partial r^2}e^{-i\Delta t(L^2/4mr^2-1/2r)}\\&\times e^{-i\Delta t\,W(r,\theta)}e^{-i\Delta t(L^2/4m^2-1/2r)}\\&\times e^{(i\Delta t/4m)\partial^2/\partial r^2}\Phi(t)+O(\Delta t^3)\ .\end{aligned} \tag{4}$$

Here, commutation errors give rise to the third-order error term in Δt. The wave function $\Phi(t)$ is generated numerically over successive time increments by repeated application of the unitary operator in Eq. (4) on the initial wave function $\Phi(t=0)$. To execute this process, the wave function $\Phi(r,\theta,\phi,t)$ is expanded in terms of spherical harmonics $\{\Psi_{lm}(\theta,\phi)\}$ and radial Fourier functions $\sin(k\pi r/R_0)$, where $r=R_0$ defines the radial grid boundary. These are, respectively, eigenfunctions of the total angular momentum operator L^2 and the radial kinetic energy operator $\partial^2/\partial r^2$. The choice of $\sin(k\pi r/R_0)$ ensures that the boundary condition $\Phi(r=0)=0$ is satisfied. Since m is a good quantum number for the systems under discussion here, the problem can be simplified by integrating over the azimuthal angle ϕ and replacing the angular momentum operator L_z with its eigenvalue m. For the sake of simplicity only the value $m=0$ is considered in the following discussion. The generalization to arbitrary values of m is discussed in Appendix A.

The application of each individual exponential operator (propagator) in the split form of the evolution opera-

tor in Eq. (4) must be preceded by a unitary transformation of basis to one that is diagonal for the operator in question. Thus the propagators containing the radial kinetic energy operator and the total angular momentum operator should be applied in radial and angular momentum space, respectively. Propagators depending on potentials, on the other hand, are applied in coordinate space on an $\{r_i,\theta_j\}$ grid.

We consider first the transformation that diagonalizes the total angular momentum operator L^2. Let us assume that the wave function can be expanded in a finite number of Legendre polynomials as

$$\Phi(r_i,x_j,t)=\sum_{l=0}^{L} f_l(r_i,t)P_l(x_j),\quad x_j=\cos\theta_j \tag{5a}$$

where the P_l are normalized Legendre polynomials or the spherical harmonics Y_{l0}. The expansion coefficients $f_l(r_i,t)$, which are functions of the radial coordinate, can be evaluated numerically by means of the Gauss-Legendre quadratures[6]

$$f_l(r_i,t)=\sum_{j=1}^{L+1} w_j P_l(x_j)\Phi(r_i,x_j,t)\ , \tag{5b}$$

where the points x_j are the $L+1$ zeros of the Legendre polynomial $P_{L+1}(x)$ and the w_j's are the corresponding quadrature weights. The use of the $L+1$ order Gauss-Legendre quadrature points and weights $\{x_j,w_j\}$ guarantees that the linear transformations of Eqs. (5a) and (5b) are exactly unitary, or equivalently

$$\delta_{l,l'}=\sum_{j=1}^{L+1} w_j P_l(x_j)P_{l'}(x_j)\ , \tag{6a}$$

$$\delta_{i,j}=w_i\sum_{l=0}^{L} P_l(x_i)P_l(x_j)\ . \tag{6b}$$

The expansion in Eq. (5a) is consequently exact at the quadrature points $\{x_j\}$ and, furthermore, the coefficients $\{f_l,\ l=0,L\}$ obtained from Eq. (5b) are equal to those that would be obtained by analytic evaluation of the integrals corresponding to Eq. (5b).

The radial functions $f_l(r,t)$, which are defined on an equidistant radial grid of N points $\{r_i;\ -R_0\le r_i \le R_0;\ r_i-r_{i-1}=2R_0/N\}$ are in turn expanded in a discrete N-term Fourier basis

$$f_l(r_j,t)=\sum_{k=-N/2+1}^{N/2} g_k(l,t)e^{\pi ikr_j/R_0}\ , \tag{7a}$$

where the coefficients are determined numerically by the trapezoid integration rule

$$g_k(l,t)=1/N\sum_{j=1}^{N} f_l(r_j,t)e^{-\pi ikr_j/R_0}\ . \tag{7b}$$

The boundary condition $\Phi(r=0,\theta,t)=0$ is guaranteed by choosing $\Phi(r,\theta,t=0)$ to be an odd function of r and employing the negative and positive r axis in the calculation. This is equivalent to expanding $\Phi(t,r,\theta)$ in terms of $\sin(k\pi r/R_0)$ but is computationally more convenient. The transformation and its inverse, defined in Eqs. (7), are also exactly unitary, since

$$\delta_{k,k'}=1/N\sum_{j=1}^{N} e^{\pi i(k-k')r_j/R_0}\ , \tag{8a}$$

$$\delta_{i,j}=1/N\sum_{k=-N/2+1}^{N/2} e^{\pi ik(r_i-r_j)/R_0}\ . \tag{8b}$$

These are well-known properties of the discrete Fourier transform and ensure that the functional representation embodied in Eqs. (7) is exact at the grid points for a band-limited function.

The application of the time-evolution operator in Eq. (4) reduces to the following steps: (i) Each Fourier expansion coefficient $g_k(l,t)$ of Eq. (7b) is multiplied by the factor

$$\exp(-i\,\Delta t\,\pi^2k^2/4mR_0^2)$$

and the inverse discrete Fourier transform, Eq. (7a) is employed to obtain the new set of radial functions $f_l(r,t)$. (ii) The second propagator from the right in Eq. (4) is applied to the expansion in Eq. (5a) and results in the multiplication of each function $f_l(r_i,t)$ by

$$\exp\{-i\,\Delta t[l(l+1)/4mr_i^2-1/2|r_i|]\}\ .$$

(iii) Eq. (5a) is then used to reconstruct the wave function $\Phi(r_i,x_j,t)$ in coordinate space. Next $\Phi(r_i,x_j,t)$ is multiplied by the interaction propagator

$$\exp[-i\,\Delta t\ W(|r_i|,x_j)]\ .$$

The resulting wave function is then reexpanded using Eq. (5b). To complete the cycle, steps (ii) and then (i) are repeated in the appropriate order.

The preceding computational procedure, although more complex than the split-operator scheme in Cartesian coordinates,[3] can be rendered computationally efficient by vectorization. In particular, the FFT operations involved in Eqs. (7a) and (7b) as well as the matrix operations involved in the transformations (5a) and (5b) and steps (i)–(iii) are vectorizable.

The numerical procedure just outlined for use in spherical coordinates parallels closely the procedure previously developed for use in Cartesian coordinates[3] in a number of respects, which it is useful to summarize here. Both methods utilize a unitary form of the evolution operator, which guarantees unconditional numerical stability and conservation of probability. In both methods the evolution operator is factored into propagators that are either functions of position or of appropriate momentum operators. Each propagator is evaluated in a representation for which it is diagonal, and the transformations that link the different representations are guaranteed to be unitary by the choice of appropriate quadratures. In both the Cartesian and spherical polar coordinate versions the numerically generated solutions, given the particular split form of the evolution operator, are in principle exact for solutions that are band-limited functions, i.e., for functions that can be represented by a finite number of Fourier and/or Legendre basis functions. In the spherical-polar-coordinate version the band-limited property in momentum space is achieved by making the grid spacing $2R_0/N$ small enough to accommodate the band-

width and by making R_0 large enough to ensure that the wave function is negligible on the radial grid boundary.

In practice, very accurate solutions can be expected if the magnitudes of the Fourier coefficients $g_k(l,t)$ are small for the largest radial momentum values represented on the grid and if the norms of the partial wave amplitudes f_l are small for the largest values of l represented in the solution (5a). During the course of the calculations both the radial and angular bandwidths of the wave function are continuously monitored to ensure that the wave function being calculated is in fact band limited. If the radial and angular spectra do not fall rapidly enough, a larger radial and/or angular basis is needed or, equivalently, a larger number of grid points in radius and/or angle is required.

The size of the time increment Δt is determined by the energy bandwidth needed to solve the problem. For a typical problem the condition $\Delta t < \pi/3\,\Delta E$ is usually sufficient, where ΔE is the maximum excursion in either the sampled potential or kinetic energies.[3]

III. SPECTRAL METHOD FOR DETERMINING ENERGY EIGENVALUES

For the convenience of the reader, we review the spectral method for calculating energy eigenvalues as developed in Ref. 3. The bound-state spectrum of a Hamiltonian can be constructed with the aid of the correlation function

$$\mathcal{P}(t)\equiv\langle\Phi(0)|\Phi(t)\rangle = \int\int\int dr\, d(\cos\theta) d\phi\, \Phi^*(r,\theta,\phi,0)\Phi(r,\theta,\phi,t) , \tag{9}$$

where the initial state $\Phi(t=0)$ can be considered a test function on the spectrum. If the time-dependent wave function is expanded as a superposition of eigenstates of the Hamiltonian

$$\Phi(t)=\sum_n a_n\psi_n(r,\theta,\phi)e^{-iE_nt} , \tag{10}$$

where

$$H\psi_n=E_n\psi_n ,$$

then the correlation function takes the form

$$\mathcal{P}(t)=\sum_n |a_n|^2 e^{-iE_nt} . \tag{11}$$

The spectral function, which is defined as the Fourier transform of the correlation function in Eq. (11),

$$\mathcal{P}(E)\equiv\int_{-\infty}^{+\infty} dt\, e^{iEt}\mathcal{P}(t) , \tag{12a}$$

$$\mathcal{P}(E)=\sum_n |a_n|^2\delta(E-E_n) , \tag{12b}$$

displays a series of resonances corresponding to the eigenvalues of the Hamiltonian. Once the eigenvalues are determined, the wave function can be constructed, apart from a normalization constant, as

$$\psi_n\sim\int_{-\infty}^{+\infty} dt\, e^{iE_nt}\Phi(t) . \tag{13}$$

The results obtained in Eq. (12b) hold for an infinite time record of the correlation function $\mathcal{P}(t)$. In practice only a finite time record of duration, T, of the correlation function is available. Consequently, the δ functions in Eq. (12b) are replaced by functions of the form $\sin[\frac{1}{2}(E-E_n)T/(E-E_n)]$, which have side lobes that could overlap or be confused with true resonances. To avoid this problem Eq. (12a) is approximated by

$$\mathcal{P}(E)=\frac{1}{T}\int_0^T dt\, w(t)e^{iEt}\mathcal{P}(t) , \tag{14}$$

where $w(t)$ is the Hanning window function given by

$$w(t)=1-\cos(2\pi t/T) \quad \text{if } 0\le t\le T .$$

When Eq. (11) is inserted into Eq. (14), the result is

$$\mathcal{P}(E)=\sum_n |a_n|^2\mathcal{L}(E-E_n) , \tag{15}$$

which also displays a series of resonances located at the energy eigenvalues. The line shape function $\mathcal{L}(E-E_n)$ is defined as

$$\begin{aligned}\mathcal{L}(E-E_n)&\equiv\frac{1}{T}\int_0^T dt\, e^{i(E-E_n)}w(t)\\ &=\frac{e^{i(E-E_n)T}-1}{i(E-E_n)T}\\ &\quad-\frac{1}{2}\left[\frac{e^{[i(E-E_n)T+2\pi]}-1}{i(E-E_n)T+2\pi}\right.\\ &\quad\left.+\frac{e^{[i(E-E_n)T-2\pi]}-1}{i(E-E_n)T-2\pi}\right] .\end{aligned} \tag{16}$$

In contrast to $\sin[\frac{1}{2}(E-E_n)T/(E-E_n)]$ the spectral line-shape function $\mathcal{L}(E-E_n)$ has no side lobes and consequently can be used for accurate identification of energy eigenvalues, provided there is no significant overlap between adjacent resonances.

The total time T limits the energy resolution of the spectral function $\mathcal{P}(E)$ to $\Delta E=2\pi/T$. At the same time the sampling interval Δt should be sufficiently small to accommodate all of the bound states and a suitable portion of the continuum by a factor of two or three.

To resolve closely spaced spectral lines, the energy grid spacing $2\pi/T$ associated with the discrete Fourier transform of the correlation function in Eq. (12a) must be smaller than the smallest energy spacing in the spectrum. Once spectral lines are resolved, a line-shape-fitting technique,[3] reviewed in Appendix B, improves the accuracy of the eigenvalue determination well beyond that prescribed in the uncertainty relation $\Delta E=2\pi/T$. This same technique also yields an accurate determination of the eigenstate probabilities $|a_n|^2$.

The corresponding eigenfunctions are calculated by an analogous modification of Eq. (13), which is

$$\frac{1}{T}\int_0^T dt\, e^{iE_nt}w(t)\Phi(t)=\sum_j a_j\psi_j\mathcal{L}(E_n-E_j) . \tag{17}$$

If the energy grid spacing $2\pi/T$ is refined enough to give good separation between the resonances, then $\mathcal{L}(E_n - E_j) \approx 0$ for $E_n \neq E_j$ and to an excellent approximation the corresponding eigenstate is given by[3]

$$\psi_n \approx \frac{1}{T}\int_0^T dt\, e^{iE_n t} w(t)\Phi(t) \; . \tag{18}$$

The test function $\Phi(t=0)$ is to some extent arbitrary; it need only contain eigenstates of interest when represented as a superposition of the complete set of states of the Hamiltonian under consideration. Sometimes symmetry considerations will govern the test function. For example, to resolve spectra corresponding to nearly degenerate eigenstates, which are differentiated on the basis of appropriate symmetry operations, the initial wave packet $\Phi(t=0)$ can be symmetrized so that any one member of a degenerate or nearly degenerate set of energy resonances is present in the spectral function $\mathcal{P}(E)$. The spectra for hydrogen in an external magnetic field, which can be labeled according to even or odd z parity, is constructed by choosing the initial wavepacket to be an even or odd function of z.

IV. APPLICATION OF THE SPLIT-OPERATOR SPECTRAL METHOD TO A HYDROGEN ATOM IN A dc ELECTRIC FIELD

The application of a dc electric field transforms the bound field-free hydrogen-atom spectrum into a continuum of ionizing states. Since perturbation-expansion techniques are known to diverge when sufficiently large fields are applied, this problem has long served as a useful test of various "exact" quantum-mechanical computational methods.[7-12] A solution of this problem would also provide a meaningful test of the accuracy and versatility of the split-operator spectral method.

If the electron is initially in the bound state ϕ_0 with energy E_0, the application of an external dc electric field will result in a mixing of the discrete state ϕ_0 with a continuum of orthogonal ionizing states $\{\phi_E\}$. Following a standard Wigner-Weisskopf treatment of the problem,[13] the energy of the discrete state is found to be shifted by an amount ΔE, and the probability of observing the system in the state ϕ_0 decays exponentially with a lifetime

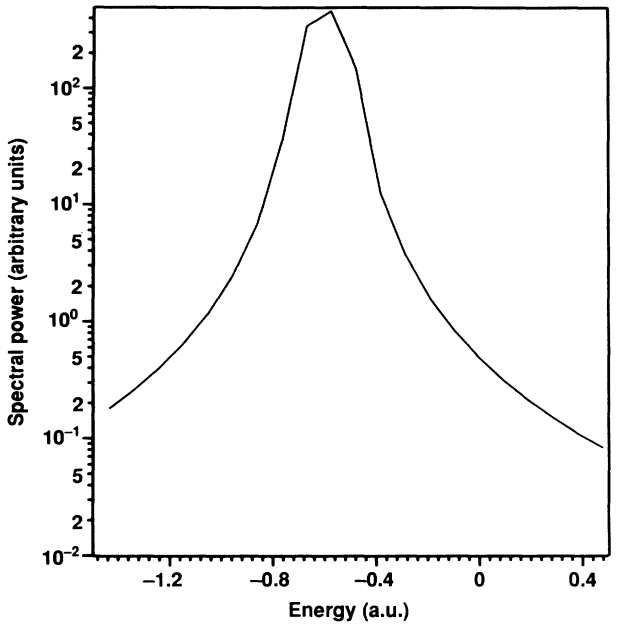

FIG. 1. Calculated energy spectrum for a hydrogen atom in a uniform static electric field. Energy corresponding to the resonant peak can be located using a line-shape-fitting technique.

Γ^{-1}. This behavior is represented by the relation

$$|\langle\phi_0|\Phi(t)\rangle|^2 = e^{-\Gamma t} \; , \tag{19}$$

where

$$\Phi(t=0) = \phi_0 \; . \tag{20}$$

The width Γ measures the distribution of final continuum states coupled to the discrete state ϕ_0.

Equation (19) can be replaced by the equivalent formal expression

$$|\langle\phi_0|e^{-iH^{\text{Stark}}t}|\phi_0\rangle|^2 = e^{-\Gamma t} \; , \tag{21}$$

where H^{Stark} is the Hamiltonian of Eq. (2) with $W(r,\theta) = W^{\text{Stark}}(r,\theta)$. If the complex eigenvalue $E_0 + \Delta E + i\Gamma/2$ is then associated with the dynamics of the discrete state ϕ_0, Eq. (21) becomes

TABLE I. Comparison of the split-operator spectral method and analytic results for hydrogen-atom Stark resonances and widths (a.u.).

F	E_R [a]	E_R [b]	$\Gamma/2$ [a]	$\Gamma/2$ [b]
0.03	−0.502 084	−0.502 074 25	0.000 000 4	0.000 000 01
0.05	−0.506 135	−0.506 195 4	0.000 038 3	0.000 038 6
0.06	−0.509 252	−0.509 203 5	0.000 247	0.000 258
0.08	−0.517 647	−0.517 56	0.002 29	0.002 30
0.10	−0.527 521	−0.527 45	0.007 32	0.007 25
0.15	−0.550 988	−0.551 20	0.0304	0.030 00
0.20	−0.570 532	−0.570 55	0.0609	0.060 45
0.25	−0.585 370	−0.5860	0.0949	0.0940

[a]These resonance energies are expressed as $E_R = 0.5 + \Delta E$, where ΔE is obtained from split-operator spectral calculations employing 4096 grid points spanning a ±80-a.u. grid.
[b]Reference 9.

$$|\langle\phi_0|e^{-i(E_0+\Delta E-i\Gamma/2)t}|\phi_0\rangle|^2=e^{-\Gamma t} . \quad (22)$$

The spectral method permits the energy shift ΔE and the width Γ to be computed in a straightforward way by the Fourier analysis of the correlation function

$$\mathcal{P}(t)\equiv\langle\Phi(0)|\Phi(t)\rangle=\langle\phi_0|e^{-iH^{\text{Stark}}t}|\phi_0\rangle , \quad (23)$$

where $\exp(-H^{\text{Stark}}t)$ in Eq. (23) is replaced by the split-operator approximation in Eq. (4).

The spectral function $\mathcal{P}(E)$ is calculated from the correlation function $\mathcal{P}(t)$ using Eq. (14). The magnitude $|\mathcal{P}(E)|$ reveals a single peak (see Fig. 1, for example), and the line-shape-fitting technique in Appendix B yields a complex resonance energy whose value can be interpreted as $E_0+\Delta E-i\Gamma/2$. The linewidth displayed in Fig. 1 is determined primarily by the record length T and is not a direct measure of the decay width Γ.

Results of split-operator spectral calculations for the Stark effect on ground-state hydrogen are given in Table I, where values of the shifted ground-state energy $E_0+\Delta E$ and half-width $\Gamma/2$ as a function of dc field strength are compared with the corresponding values from Ref. 9. The spectral-method results in Table I were obtained using a time step of duration 0.002 a.u. and 4096 radial points spanning a grid from -80 to $+80$ a.u. and a 14-term angular expansion. In general the size of the grid is dictated by the requirement that the wave packet be negligible on the grid boundary to avoid spurious effects introduced by the imposition of periodic boundary conditions. In cases where ionization is involved the wave packet must eventually hit the boundary. To prevent boundary reflections a pure imaginary short-range contribution, which is appreciable only near the boundary, is added to the potential. This imaginary contribution to the potential acts as an absorber. It has been established that the energy shift ΔE and the decay width Γ are quite insensitive to the exact form of this absorber.

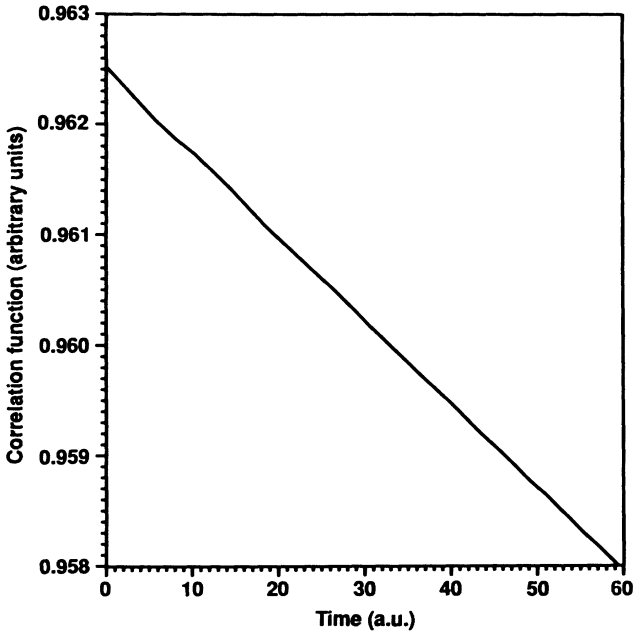

FIG. 2. Absolute value of the correlation function corresponding to Fig. 1. Measurement of time is begun well after adiabatic turn-on of the electric field.

The electric field was turned on adiabatically and the exponential decay of the initial state was allowed to develop, typically over 4000 to 10 000 time steps. After exponential decay of the initial state had been established, the correlation function and spectrum were computed, typically over an additional 4000 time steps. Figure 2 shows a plot of the absolute value of the correlation function corresponding to Fig. 1 for a field strength $F=0.05$

TABLE II. Convergence of Stark resonances and widths for hydrogen atom in calculations with the split-operator spectral method. (All values in a.u.)

			E_0 [a]	$(E_r$ [b], $\Gamma/2)$			
n_r	$\pm R_0$	$L_{\max}$	$F=0$	$F=0.05$		$F=0.1$	
1024	80		0.492 75				
1024	80	4		0.506 47	0.000 051 9	0.528 71	0.008 09
1024	80	6		0.506 47	0.000 051 6	0.528 73	0.008 13
1024	80	10		0.506 47	0.000 0515	0.528 73	0.008 13
1024	80	14		0.506 47	0.000 051 5	0.528 73	0.008 13
2048	80		0.498 06				
2048	80	4		0.506 21	0.000 041 9	0.527 77	0.007 46
2048	80	6		0.506 21	0.000 041 6	0.527 78	0.007 51
2048	80	10		0.506 21	0.000 041 7	0.527 78	0.007 51
2048	80	14		0.506 21	0.000 041 7	0.527 78	0.007 51
4096	80		0.499 49				
4096	80	4		0.506 13	0.000 056 3	0.527 49	0.007 22
4096	80	6		0.506 13	0.000 041 3	0.527 56	0.007 30
4096	80	10		0.506 14	0.000 039 4	0.527 54	0.007 32
4096	80	14		0.506 14	0.000 038 3	0.527 52	0.007 32

[a]Binding energy for 1s state of field-free hydrogen.
[b]$E_R=0.5+\Delta E$.

a.u. For this relatively low field, exponential decay of the initial state takes a relatively long time to develop as can be seen from the small undulations in the upper part of the curve. The field was turned on over 2000 time steps, and the correlation function begins after 20 000 steps. For this case, the complex eigenvalue that appears in Table I was computed from the last quarter of the correlation function.

The resonance energies and decay widths calculated by the split-operator spectral method are in good agreement with their analytic counterparts in Table I. The resonance energies, which generally agree to four significant figures, are in better agreement than the decay times due to the necessity for avoiding transient effects for accurate calculation of the decay times.

Table II shows the convergence of results for two different field strengths as a function of radial zoning and the number of spherical harmonics included in the calculation. Also given in Table II are field-free ground-state energies E_0 for hydrogen. Since the 1s state is spatially compact and concentrated close to the origin, its calculated energy is quite sensitive to the numerical representation of the Coulomb potential on the grid. When sufficiently small grid spacings are employed, however, accurate spectra and eigenvalues can be generated.

These calculations of field ionization in hydrogen suggest that the split-operator spectral method has sufficient accuracy to describe the field ionization of hydrogen from high Rydberg states by microwave fields[14,15] as well as the multiphoton ionization of hydrogen by laser fields.[16] The present method is, moreover, uniquely suited for describing ionization processes where a well-defined short pulse of radiation is involved.

V. SPLIT-OPERATOR METHOD IN THE STRONG-MAGNETIC-FIELD LIMIT

The split-operator method developed for use in spherical coordinates in Sec. II is appropriate for treating a hydrogen atom in a magnetic field provided the magnetic interaction energy is small compared to the Coulomb binding energy, since accurate computations can be performed with a reasonable number of terms in the angular expansion. When the magnetic interaction energy is comparable to or exceeds the Coulomb binding energy, the number of terms in the angular expansion can become excessive, and it becomes more efficient to employ cylindrical coordinates. The Hamiltonian for a hydrogen atom in a strong magnetic field can be written in cylindrical coordinates and atomic units as

$$H=h_0-\frac{1}{2m}\frac{\partial^2}{\partial z^2}-\frac{1}{(\rho^2+z^2)^{1/2}} . \tag{24}$$

Here, h_0 is the two-dimensional Hamiltonian describing the electron motion in the plane perpendicular to the magnetic field and is given by

$$h_0=-\frac{1}{2m}\left[\frac{1}{\rho}\frac{\partial}{\partial\rho}\rho\frac{\partial}{\partial\rho}+\frac{1}{\rho}\frac{\partial^2}{\partial\phi^2}\right] -\frac{1}{2m}i\beta\frac{\partial}{\partial\phi}+\frac{1}{8m}\beta^2\rho^2 , \tag{25}$$

where $\beta=\alpha B$ is the magnetic field strength parameter in atomic units.

The time-dependent wave function is advanced over one time increment in the split-operator approximation by the formal expression

$$\Phi(t+\Delta t)=e^{(i\Delta t/4m)\partial^2/\partial z^2}e^{-i\Delta t h_0/2} \times e^{-i\Delta t/(\rho^2+z^2)^{1/2}}e^{-i\Delta t h_0/2} \times e^{(i\Delta t/4m)\partial^2/\partial z^2}\Phi(t) . \tag{26}$$

The procedure for propagating the wave function one time increment is analogous to that described in Sec. II. The time-dependent wave function $\Phi^m(z,\rho,t)$ (the ϕ degree of freedom is integrated out) for a particular value of the quantum number m is numerically evaluated on an appropriate coordinate grid $\{z_i,\rho_j\}$ and then expanded in terms of the eigenfunctions of h_0

$$\Phi^m(z_i,\rho_j,t)=\sum_{n=0}^{N} f_n(z_i,t)\chi_{nm}(\rho_j) , \tag{27}$$

where

$$h_0\chi_{nm}(\rho)=\beta(n+\tfrac{1}{2}m+\tfrac{1}{2}|m|+\tfrac{1}{2})\chi_{nm}(\rho) . \tag{28}$$

Here the functions χ_{nm} are the so-called Landau functions which can be explicitly written as[17]

$$\chi_{nm}(\rho)=\left[\frac{2\beta n!}{(n+|m|)!}\right]^{1/2} e^{-\beta\rho^2/2}(\beta\rho^2)^{|m|/2}L_n^{|m|}(\beta\rho^2) \tag{29}$$

and satisfy the orthogonality relation

$$\int_0^\infty \chi_{nm}(\rho)\chi_{n'm}(\rho)\rho\,d\rho=\delta_{n,n'} . \tag{30}$$

Since the Landau orbitals can be expressed in terms of the Laguerre polynomials $L_n^{|m|}$, the expansion coefficients can be evaluated exactly by appropriate Gauss-Laguerre quadratures as

$$f_n(z,t)=(2\beta)^{-1}\sum_{j=1}^{N+1} w_j\chi_{nm}(\rho_j)\Phi(z,\rho_j,t)e^{\beta\rho_j^2} \times(\beta\rho_j^2)^{-|m|} . \tag{31}$$

Here $\{\rho_j/\beta)^{1/2},w_j\}$ are the $N+1$-order Gauss-Laguerre quadrature points and weights. Since the appropriate Laguerre quadrature points are employed in the construction of the expansion coefficients of Eq. (31), the transformations and inverse transformations from Landau functional space to coordinate space [i.e., Eq. (27) and Eq. (31)] are exactly unitary,

$$\delta_{n,n'}=\sum_{j=1}^{N+1} w_j\chi_{nm}(\rho_j)\chi_{n'm}(\rho_j) , \tag{32a}$$

$$\delta_{i,j}=w_i\sum_{n=0}^{N}\chi_{nm}(\rho_i)\chi_{nm}(\rho_j) . \tag{32b}$$

The expansion coefficients $f_n(z,t)$ are expressed as Fourier series in z and are evaluated in a manner that closely parallels the evaluation of the $f_l(r,t)$ in Sec. II.

VI. NUMERICAL RESULTS FOR A HYDROGEN ATOM IN A UNIFORM MAGNETIC FIELD

The theoretical description of a hydrogen atom in a uniform magnetic field is one of the basic nonseparable problems of atomic physics and has as a consequence attracted wide interest. The development of methods for treating this problem over a wide range of field strengths, including immediate field strengths, where the Coulomb and magnetic field strengths become comparable, has proven to be a significant challenge.[18]

As an additional test of the versatility and accuracy of the split-operator spectral method it has been used to determine the effect of magnetic fields of varying strength on the lowest energy levels of hydrogen. Calculational results are presented for both spherical harmonic and Landau basis expansions in Table III, where they are compared with some of the extensive results obtained by Rösner *et al.*,[19] using an adaptation of a Hartree-Fock method by Froese-Fischer.[20] The energies of the states in Table III are designated by their zero-field-limit quantum labels and their z parity ($\pm$). The results obtained by Rösner *et al.* are assumed to be accurate in all the significant figures listed.

Computations with the spherical harmonic basis were performed with 10 to 12 spherical harmonics for the lowest magnetic fields and up to 40 for higher fields. Typical calculations with the Landau basis were performed with a 40-term expansion. For the spherical harmonic basis calculations, a 30 a.u. grid with 1024 to 2048 radial increments was used. Typical calculations were performed using 16 000 time increments. Although some effort was made to adjust the numerical parameters of the problem to improve accuracy, no attempt was made to optimize them. In addition, no effort was made to systematically study the convergence in accuracy as a function of the number of expansion terms. Energy eigenvalues for this problem could be computed from a somewhat arbitrary set of initial wave functions as long as the one used possessed the chosen parity and m value. We chose a linear combination of field-free hydrogen orbitals with

TABLE III. Electron binding energies for a hydrogen atom in a uniform magnetic field. Comparison between results obtained using the split-operator spectral method and results from Ref. 15. The former are obtained using both a spherical harmonic and a Landau basis.

γ[a]	Spherical	Landau	Rösner *et al.*	Spherical	Landau	Rösner *et al.*
	$2p$ $m=0$ $(-)$				$3p$ $m=0$ $(-)$	
0.005	0.129 86		0.129 85	0.059 692		0.059 688
0.05	0.162 42	0.161 81	0.162 41	0.069 897	0.069 661	0.069 892
0.5	0.260 06	0.259 94	0.260 01	0.090 182	0.090 210	0.0902
2	0.334 24	0.335 66	0.335 70	0.098 234	0.102 94	0.102 95
5		0.382 57	0.383		0.109 83	0.109 85
10		0.413 20	0.413 38		0.114 02	0.114 05
50		0.463 59	0.463 62		0.121 29	0.120 52
	$2p$ $m=1$ $(+)$				$3p$ $m=1$ $(+)$	
0.005	0.134 71		0.134 701	0.063 824		0.063 820
0.05	0.200 86		0.200 846	0.081 180		0.081 171
0.5	0.456 86	0.456 31	0.456 597	0.125 44	0.125 44	0.125 461
2	0.793 77	0.787 55	0.787 826	0.154 99	0.159 69	0.1597
5		1.1244	1.125 42		0.182 25	0.1823
10		1.4633	1.4655		0.198 77	0.198 862
50		2.6326	2.635		0.230 10	0.234 752
	$3d$ $m=1$ $(-)$				$4d$ $m=1$ $(-)$	
0.005	0.064 68		0.064 678 2	0.038 132		0.038 132 2
0.05	0.107 81		0.107 812 1	0.053 244		0.053 245 7
0.5	0.206 48	0.206 57	0.206 567 4	0.079 022	0.079 320	0.079 359 4
2	0.282 37	0.285 80	0.285 802 7	0.082 371	0.094 681	0.094 698 7
5		0.338 95	0.338 956 1		0.103 37	0.103 354 0
10		0.376 11	0.376 119 8		0.108 83	0.108 853 7
50		0.442 79	0.442 871 2		0.117 87	0.117 880 9
	$1s$ $(+)$				$2s$ $(+)$	
0.005	0.505 04		0.504 975 0	0.129 59		0.129 651 6
0.05	0.547 53		0.547 526 5	0.147 99		0.148 089 2
0.5	0.830 95		0.831 168 0	0.158 37		0.160 469 0
2	1.2796		1.280 798	0.187 71		0.188 81
5	1.7445	1.7294	1.747 797	0.192 60	0.209 11	0.208 89
10	2.2082	2.1586	2.215 399	0.214 94	0.222 25	0.223 81
50		3.4925	3.789 05		0.251 33	0.256 169 5

[a] $\gamma = B/2c = (2.12715 \times 10^{-10}\ \text{a.u.}/G)B(G)$.

the specified parity and m value. The resulting spectra displayed one or more resonances, and the energies corresponding to the lowest lying resonance in the appropriate spectrum are listed in Table III.

The agreement between the split-operator spectral calculations and the results of Rösner *et al.* is in general quite good and is frequently to four significant figures. As would be expected, the table shows that split-operator results are most accurate for the spherical harmonic basis when the field strength is weak and most accurate for the Landau basis when the field is strong. This follows from the fact that for small magnetic fields the electron motion is determined mainly by the spherically symmetric Coulomb force, while for large fields the electron dynamics is dominated by the magnetic field. For intermediate fields the Coulomb and magnetic field energies can be comparable, and accuracy requires large expansion sets in either basis. Table III also shows slightly poorer accuracy for the spatially compact $1s$ state than for higher states, which results from sensitivity of that state to the sampling of the singular Coulomb potential on the numerical grid.

VII. CALCULATION OF DIPOLE PHOTO ABSORPTION SPECTRA IN ATOMIC HYDROGEN USING THE SPLIT-OPERATOR SPECTRAL METHOD

The experimental generation of photoabsorption spectra of atoms in strong external fields has become a topic of considerable interest.[21,22] The split-operator spectral method offers some interesting possibilities for understanding these spectra and in this section we consider the task of generating them. But in the interest of evaluating the accuracy of the method we restrict our attention to the generation of photoabsorption spectra for field-free hydrogen in the low intensity, i.e., single-photon dipole limit, where first-order perturbation theory provides analytic results for comparison.

It can be shown that the dipole photoabsorption cross section can be computed from the Fourier transform of the dipole correlation function.[23] This method is easily implemented using a split-operator propagator and the numerical spectral-analysis technique described in Sec. III and Appendix B.

The dipole correlation function can be expressed as

$$\langle \Phi(0)|\Phi(t)\rangle \equiv \langle \psi_0|\mu e^{-H^0 t}\mu|\psi_0\rangle \ , \tag{33}$$

where ψ_0 is the initial Coulomb state with energy E_0, H^0 is the field-free Coulomb Hamiltonian, μ is the dipole operator, and the propagator $e^{-iH^0 t}$ is approximated by the unitary split operator given in Eq. (4) with $W(r,\theta)=0$. Equation (33), it will be noted, has the form of the overlap of a wave packet at time t on the same wave packet at time $t=0$, as in Eq. (9). A numerical evaluation of the photoabsorption cross section in the electric dipole approximation can be obtained by evaluating the integral

$$\sigma(E-E_0)=[(4\pi^2 a_0^2(E-E_0)/T)] \times \int_0^T dt\, w(t) e^{iEt}\langle \Phi(0)|\Phi(t)\rangle \ , \tag{34}$$

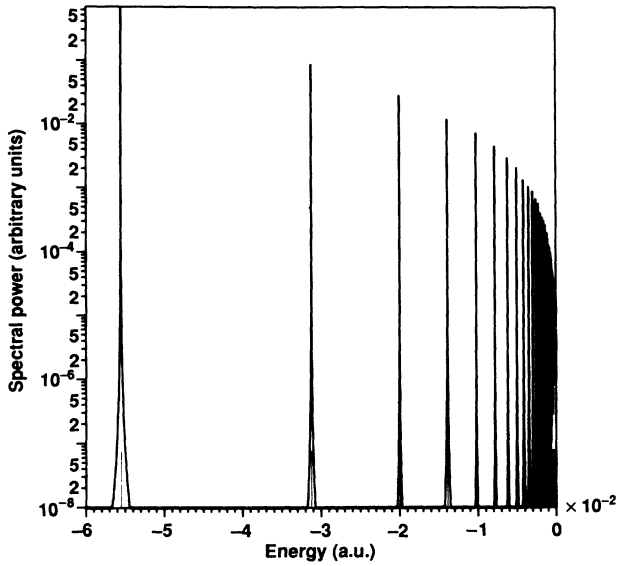

FIG. 3. Calculated energy spectrum for $2p$-nd bound-bound transitions. Positions of peaks indicate final transition energies, and heights of peaks are a measure of oscillator strengths. Large tick marks indicate analytic values of energies. Resonances start with $n=3$.

where E is the final-state energy. Expression (34) has the form of the energy spectrum (14).

The final-state energies E_j are obtained from the location of the peaks of the spectral function (34), and the corresponding dipole oscillator strengths

$$f_{0\to j}=2m(E_j-E_0)|\langle \psi_0|\mu|\psi_j\rangle|^2 \tag{35}$$

are determined from the heights of the resonant peaks of the spectrum using the technique outlined in Appendix B. In general, this method can be expected to apply not

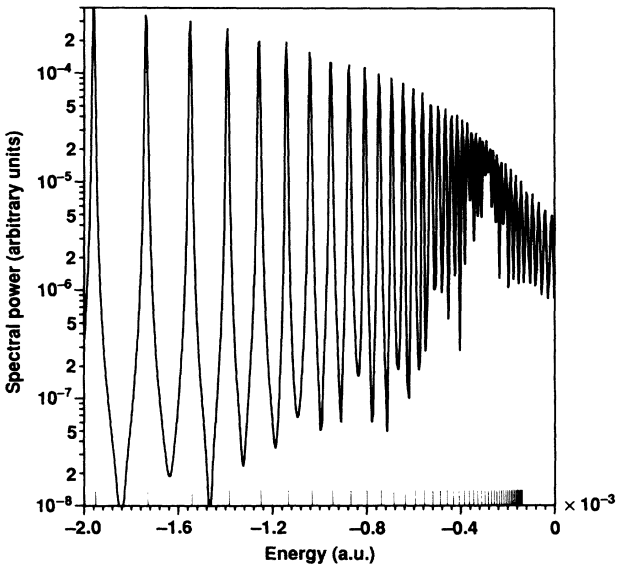

FIG. 4. Close-up of the energy spectrum shown in Fig. 3. Resonances start with $n=16$.

only to bound-bound transitions, but to transitions involving resonant states in the continuum as well, as was demonstrated by the results for the Stark effect on hydrogen in Sec. IV.[24] The spectrum of a hydrogen atom in a strong magnetic field exhibits a structure rich in above-threshold ionization levels due to the tight confinement of the electron by the magnetic field. A treatment of these levels will be described in a future publication.

The dipole photoabsorption spectrum for light polarized in the z direction has been calculated for the $2p$-$nd(m=1)$ channel in field-free hydrogen and is exhibited in Figs. 3 and 4. The initial wave packet was assumed to have the form $z\psi_{2p}$, where ψ_{2p} is the $2p$ orbital of hydrogen. Figure 3 shows the complete spectrum generated by the calculation below the ionization limit, and Fig. 4 shows a detailed plot of the spectrum in the energy range between -2×10^{-3} a.u. and the ionization limit. Tick marks on the horizontal scale indicate the analytically derived energy levels. Resonances in Fig. 3 start with $n=3$ and in Fig. 4 start with $n=16$. A comparison between the final-state energy levels and oscillator strengths, calculated with the split-operator spectral method and from analytic formulas,[25] is presented in Table IV. Figure 5 shows contours of equal probability

TABLE IV. Comparison between split-operator spectral method (SOSM) and analytic (A) values for field-free hydrogen-atom $\Psi_{2p}\rightarrow\Psi_{nd}$ transition. Indicated are final-state energies E_n and oscillator strengths. Numbers in square brackets denote powers of ten.

n	E_n		$f_{0\rightarrow n}$	
	SOSM	A	SOSM	A
3	0.555 46[−1]	0.555 56[−1]	0.695 76[−1]	0.695 78[−1]
4	0.312 46[−1]	0.312 50[−1]	0.121 88[−1]	0.121 80[−1]
5	0.199 98[−1]	0.200 00[−1]	0.444 16[−2]	0.443 70[−2]
6	0.138 88[−1]	0.138 89[−1]	0.216 55[−2]	0.216 29[−2]
7	0.102 03[−1]	0.102 04[−1]	0.123 47[−2]	0.123 31[−2]
8	0.781 20[−2]	0.781 25[−2]	0.776 70[−3]	0.775 64[−3]
9	0.617 25[−2]	0.617 28[−2]	0.522 79[−3]	0.522 05[−3]
10	0.499 97[−2]	0.500 00[−2]	0.369 82[−3]	0.369 28[−3]
11	0.413 20[−2]	0.413 22[−2]	0.271 78[−3]	0.271 38[−3]
12	0.347 21[−2]	0.347 22[−2]	0.205 87[−3]	0.205 56[−3]
13	0.295 85[−2]	0.295 86[−2]	0.159 84[−3]	0.159 60[−3]
14	0.255 09[−2]	0.255 10[−2]	0.126 67[−3]	0.126 48[−3]
15	0.222 21[−2]	0.222 22[−2]	0.102 14[−3]	0.101 99[−3]
16	0.195 31[−2]	0.195 31[−2]	0.835 98[−4]	0.834 70[−4]
17	0.173 00[−2]	0.173 01[−2]	0.693 10[−4]	0.692 03[−4]
18	0.154 32[−2]	0.154 32[−2]	0.581 17[−4]	0.580 26[−4]
19	0.138 50[−2]	0.138 50[−2]	0.492 21[−4]	0.491 44[−4]
20	0.125 00[−2]	0.125 00[−2]	0.420 59[−4]	0.419 93[−4]
21	0.113 38[−2]	0.113 38[−2]	0.362 27[−4]	0.361 71[−4]
22	0.103 30[−2]	0.103 31[−2]	0.314 27[−4]	0.313 80[−4]
23	0.945 16[−3]	0.945 18[−3]	0.274 48[−4]	0.274 03[−4]
24	0.868 04[−3]	0.868 06[−3]	0.241 06[−4]	0.240 72[−4]
25	0.799 98[−3]	0.800 00[−3]	0.212 92[−4]	0.212 62[−4]
26	0.739 63[−3]	0.739 64[−3]	0.189 05[−4]	0.188 73[−4]
27	0.685 86[−3]	0.685 87[−3]	0.168 63[−4]	0.168 30[−4]
28	0.637 74[−3]	0.637 76[−3]	0.151 03[−4]	0.150 73[−4]
29	0.594 52[−3]	0.594 53[−3]	0.135 72[−4]	0.135 52[−4]
30	0.555 55[−3]	0.555 56[−3]	0.122 43[−4]	0.122 30[−4]
31	0.520 29[−3]	0.520 29[−3]	0.110 74[−4]	0.110 74[−4]
32	0.488 25[−3]	0.488 28[−3]	0.101 09[−4]	0.100 60[−4]
33	0.459 16[−3]	0.459 14[−3]	0.921 81[−5]	0.916 65[−5]
34	0.432 52[−3]	0.432 53[−3]	0.836 94[−5]	0.837 58[−5]
35	0.408 15[−3]	0.408 16[−3]	0.766 73[−5]	0.767 35[−5]
36	0.385 78[−3]	0.385 80[−3]	0.707 39[−5]	0.704 78[−5]
37	0.365 20[−3]	0.365 23[−3]	0.651 61[−5]	0.648 83[−5]
38	0.346 25[−3]	0.346 26[−3]	0.596 69[−5]	0.598 66[−5]
39	0.329 50[−3]	0.328 73[−3]	0.607 47[−5]	0.553 54[−5]
40	0.313 32[−3]	0.312 50[−3]	0.566 97[−5]	0.512 85[−5]
41	0.296 69[−3]	0.297 44[−3]	0.530 75[−5]	0.476 06[−5]
42	0.283 15[−3]	0.283 45[−3]	0.446 59[−5]	0.442 70[−5]
43	0.269 17[−3]	0.270 42[−3]	0.416 69[−5]	0.412 40[−5]
44	0.254 13[−3]	0.258 26[−3]	0.390 58[−5]	0.384 80[−5]
45	0.237 46[−3]	0.246 91[−3]	0.364 64[−5]	0.359 61[−5]

at various times for the wave packet used to generate the spectra in Figs. 3 and 4.

The numerical results summarized in Figs. 3 and 4 and tabulated in Table IV were obtained using 4096 radial grid points spanning the range between -4000 and 4000 a.u. and two angular states, corresponding to $l=1$ and $m=1$ and $l=2$ and $m=1$. The calculation was run a total of $2^{20}\approx 10^6$ time steps of duration $\Delta t=1.1$ a.u., which defines an energy grid resolution of $\Delta E\cong 5\times 10^{-6}$ a.u.

It is seen from Table IV that numerically determined energies agree with analytic values to four significant figures through $n=38$, but accuracy declines after that. Numerical oscillator strengths, on the other hand, agree with their analytic counterparts for the most part to three significant figures but decline in accuracy for n values slightly lower than $n=38$. The loss in accuracy of both energies and oscillator strengths at the highest n values can be attributed both to the increasing overlap of the spectral lines and to the encroachment of the highest Rydberg states on the grid boundary. In any case, the overall accuracy of the representation of the Rydberg states out to $n=38$ is remarkable in view of the course spacing of the radial grid, which is approximately 2 a.u. It is clear that the number of time steps required to analyze a given Coulomb or Coulomb-like level scheme must rise rapidly with the number of levels required. The fact that the method can be used to generate accurate solutions to problems requiring in excess of a million integration steps, is an impressive demonstration of the stability and overall accuracy of the method.

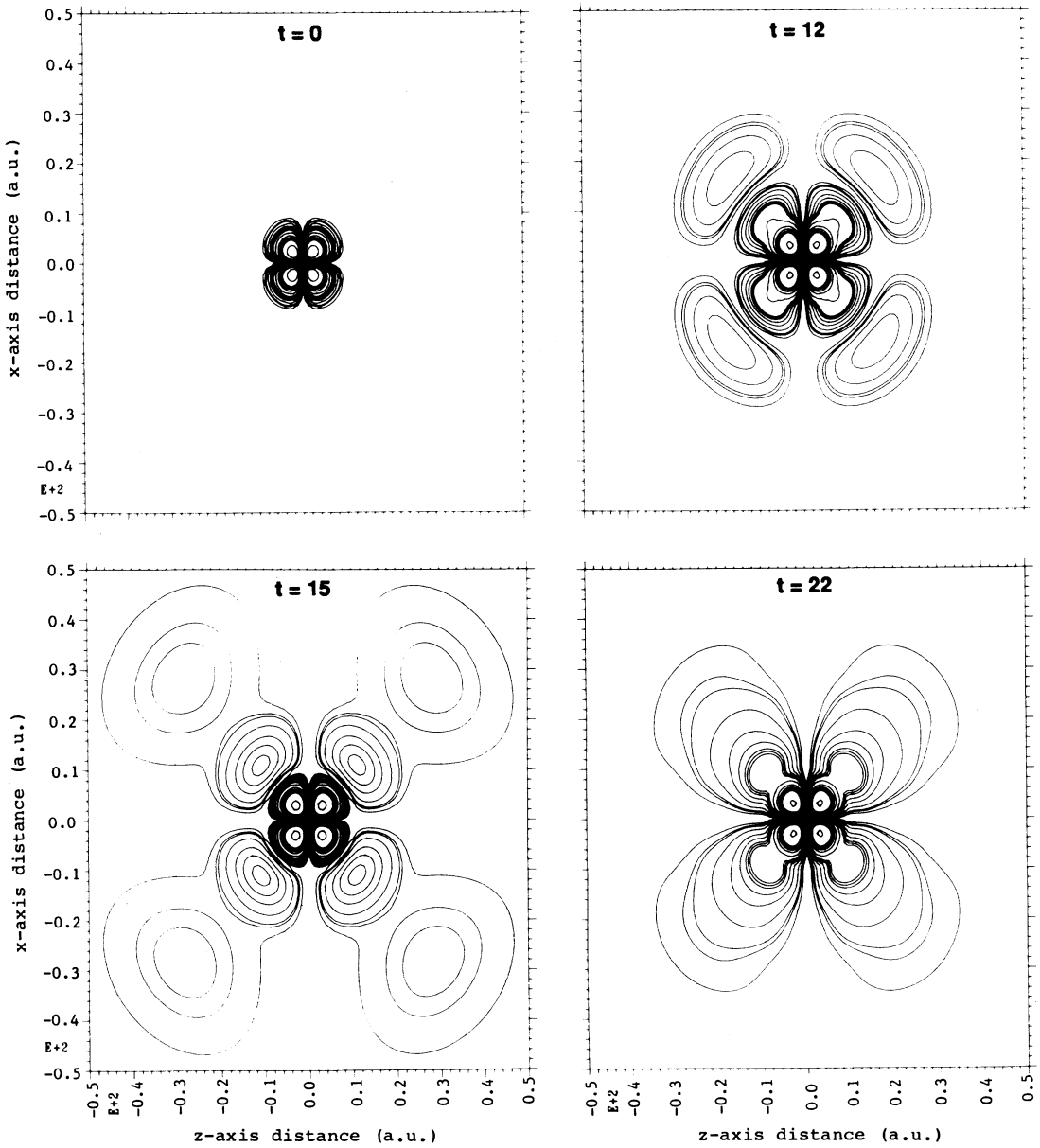

FIG. 5. Contours of equal probability calculated from the wave packet used to generate the spectra in Figs. 3 and 4. Times are indicated in units of 2000 a.u.

VIII. SUMMARY AND CONCLUSIONS

We have generalized to spherical coordinates the split-operator spectral method previously developed for Cartesian coordinates. This generalization is based on an expansion of the wave function as a Fourier series in the radial coordinate and Legendre functions in the polar angle. The use of Gauss quadratures in the evaluation of the angular expansion coefficients permits the high degree of accuracy and stability that has already been demonstrated for the method in Cartesian coordinates.

The method is applicable to explicitly time dependent problems or to the determination of the stationary states of quantum mechanical systems. In this paper the latter application was emphasized to demonstrate both the accuracy and versatility of the method.

We have shown that the method is applicable to problems involving ionization and the effects of large external electric or magnetic fields on hydrogen. We have also demonstrated that the method gives an accurate description of high Rydberg states of hydrogen. Our results will form the basis for future applications to high Rydberg states in external fields as well as the interaction of short intense laser pulses with atoms and molecules.

ACKNOWLEDGMENTS

This work was performed under the auspices of the U. S. Department of Energy by the Lawrence Livermore National Laboratory under Contract No. W-7405-ENG-48.

APPENDIX A: NUMERICAL EVALUATION OF ANGULAR EXPANSION COEFFICIENTS WHEN $m \neq 0$

The time-dependent wave function $\Phi^m(r,\theta,t)$ for a particular value of m is obtained by expanding the total wave function in spherical harmonics (Y_{lm}), and integrating over the azimuthal angle ϕ, which results in

$$\Phi^m(r,x,t)=\sum_{l=m}^{L+1} f_l(r,t)P_l^m(x), \quad x=\cos\theta \tag{A1a}$$

where the expansion coefficients are given by

$$f_l(r,t)=\int_{-1}^{+1} dx\, P_l^m(x)\Phi^m(r,x,t) . \tag{A1b}$$

Here P_l^m are the normalized associated Legendre functions.

The numerical stability and accuracy of the formulation outlined in Sec. II for $m=0$ are a consequence of the orthogonality relations in Eqs. (6), which result from the use of appropriate quadrature points and weights and related orthogonal polynomials. The same task can be accomplished for the associated Legendre functions by expressing them in terms of Jacobi orthogonal polynomials[6] and employing Gauss-Jacobi quadratures to evaluate Eq. (A1b). The required relationship is

$$P_{n+m}^m(x)=(1-x^2)^{m/2}J_n^{(m,m)}(x), \quad n=0,1,\ldots \tag{A2}$$

where $J_n^{(m,m)}$ are the normalized Jacobi polynomials, which satisfy

$$\delta_{n,n'}=\int_{-1}^{+1} dx\, J_n^{(m,m)}(x)J_{n'}^{(m,m)}(x)(1-x^2)^m . \tag{A3}$$

In the special case of $m=0$ the Jacobi polynomials reduce to the Legendre polynomials.

Inserting expression (A2) into Eq. (A1a) gives

$$\Phi^m(r,x_j,t)=\sum_{n=0}^{L} f_n^m(r,t)J_n^{(m,m)}(x_j)(1-x_j^2)^{m/2} , \tag{A4a}$$

where the expansion coefficients are obtained from Gauss-Jacobi quadratures as

$$f_n^m(r,t)=\sum_{j=1}^{L+1} w_j J_n^{(m,m)}(x_j)\Phi^m(r,x_j,t)(1-x_j^2)^{-m/2} . \tag{A4b}$$

Here $\{x_j,w_j\}$ are the related $L+1$-order Gauss-Jacobi quadrature points and weights. The use of the Jacobi orthogonal polynomials and related Gauss-Jacobi quadratures guarantee that the linear transformations of Eqs. (A4) are exactly unitary,

$$\delta_{n,n'}=\sum_{j=1}^{L+1} w_j J_n^{(m,m)}(x_j)J_{n'}^{(m,m)}(x_j) , \tag{A5a}$$

$$\delta_{i,j}=w_i\sum_{n=0}^{L} J_n^{(m,m)}(x_i)J_n^{(m,m)}(x_j) . \tag{A5b}$$

Consequently, for a band-limited function the expansion coefficients $f_n^m(r,t)$ are equivalent to those obtained from analytic evaluation of Eq. (A1b). The remainder of the formulation is identical to that outlined in Sec. II.

APPENDIX B: LINE-SHAPE-FITTING METHOD

The line-shape function $\mathcal{L}(E-E_n)$ can be written

$$\mathcal{L}(\delta)=\mathcal{F}(\delta)-\tfrac{1}{2}[\mathcal{F}(\delta+1)+\mathcal{F}(\delta-1)] , \tag{B1}$$

where

$$\mathcal{F}(\delta)=[\exp(2\pi i\delta)-1]/2\pi i\delta, \quad \mathcal{F}(0)=1 , \tag{B2}$$

and

$$\delta=(E-E_n)T/2\pi . \tag{B3}$$

Let us assume that a local maximum in the sampled values of $\mathcal{P}(E)$ occurs for $E_m=m\,\Delta E$, where ΔE is the sampling interval in the computation of the numerical Fourier transform $\mathcal{P}(E)$. In the range $(m-1)\Delta E \leq E \leq (m+1)\Delta E$, $\mathcal{P}(E)$ can, to an excellent approximation, be represented as

$$\mathcal{P}(E)=W_n\mathcal{L}(E-E_n) , \tag{B4}$$

where E_n is the desired eigenvalue. Let the following ratio be formed from sampled values of $\mathcal{P}(E)$ in the neighborhood of E_m,

$$R=\mathcal{P}[(m+1)\Delta E]/\mathcal{P}[(m-1)\Delta E] =\mathcal{L}(\delta'+1)/\mathcal{L}(\delta'-1) , \tag{B5}$$

where

$$\delta'=E_m-E_n)T/2\pi . \tag{B6}$$

Making use of Eqs. (B2) and (B3), we can write Eq. (B5) as

$$(\delta'^2-3\delta'+2)/(\delta'^2+3\delta'+2)=R \ , \tag{B7}$$

or equivalently

$$\delta'^2-3\delta' r+2=0 \ , \tag{B8}$$

where

$$r=(1+R)/(1-R) \ . \tag{B9}$$

The solutions to Eq. (B8) are

$$\delta'=[3r\pm(9r^2-8)^{1/2}]/2 \ . \tag{B10}$$

The correct solution is the one which satisfies $-\frac{1}{2}\leq \mathrm{Re}\delta \leq \frac{1}{2}$. In terms of the line-center offset parameter δ', E_n then can be determined from

$$E_n=E_m-2\pi\delta'/T \ , \tag{B11}$$

and $W_n=|a_n|^2$, the weight of the state n in the wave packet, can be obtained from

$$W_n=\mathcal{P}(m\,\Delta E)/\mathcal{L}(\delta') \ . \tag{B12}$$

[1]K. Kulander, Phys. Rev. A **35**, 445 (1987); **36**, 2726 (1987).

[2]W. P. Reinhardt, J. Phys. B **16**, L635 (1983).

[3]M. D. Feit, J. A. Fleck, Jr., and A. Steiger, J. Comput. Phys. **47**, 412 (1982).

[4]M. D. Feit and J. A. Fleck, Jr., J. Chem. Phys. **78**, 301 (1983).

[5]M. D. Feit and J. A. Fleck, Jr., J. Chem. Phys. **80**, 2578 (1984).

[6]*Handbook of Mathematical Functions with Formulas, Graphs, and Mathematical Tables,* edited by M. Abromowitz and I. A. Stegun (U. S. GPO, Washington, D. C., 1964).

[7]M. H. Alexander, Phys. Rev. **178**, 34 (1969).

[8]J. O. Hirschfelder and L. A. Curtiss, Phys. Rev. **55**, 1395 (1972).

[9]M. Henberger, H. V. McIntosh, and Erkki Brandas, Phys. Rev. A **10**, 1494 (1974).

[10]E. Luc-Koenig and A. Bachelier, J. Phys. B **13**, 1743 (1980).

[11]A. Maquet, Shih-I Chu, and W. P. Rheinhardt, Phys. Rev. A **27**, 2946 (1983).

[12]V. V. Kolosov, J. Phys. B **20**, 2359 (1987).

[13]V. Weisskopf and E. Wigner, Z. Phys. **63**, 54 (1930); **65**, 18 (1930).

[14]See, for example, R. R. Freeman and N. P. Economu, Phys. Rev. A **20**, 2356 (1979).

[15]See, for example, J. E. Bayfield and L. A. Pinnaduwage, Phys. Rev. Lett. **54**, 313 (1985).

[16]See, for example, S. I. Chu and J. C. Cooper, Phys. Rev. A **22**, 2769 (1985).

[17]L. D. Landau and E. M. Lifschitz, *Quantum Mechanics* (Pergamon, New York, 1977) p. 459.

[18]For a review see, for example, C. W. Clark, K. T. Lu, and A. F. Starace, in *Progress in Atomic Spectroscopy, Part C,* edited by M. J. Beyer and J. Kleinpoppen (Plenum, New York, 1984), pp. 247–320.

[19]W. Rösner, G. Wunner, H. Herold, and H. Ruder, J. Phys. B **17**, 29 (1984).

[20]C. Froese-Fischer, *The Hartree-Fock Method for Atoms: A Numerical Approach* (Wiley, New York, 1977).

[21]D. Klepner, M. G. Littman, and M. L. Zimmerman, in *Rydberg States of Atoms and Molecules,* edited by R. F. Stebbings and F. B. Dunning (Cambridge University Press, Cambridge, 1983), pp. 73–116.

[22]J. Main, G. Wiebusch, A. Holle, and K. H. Welge, Phys. Rev. Lett. **57**, 2789 (1986).

[23]See, for example, U. Fano, and J. W. Cooper, Rev. Mod. Phys. **40**, 441 (1968); E. J. Heller, J. Chem. Phys. **68**, 2066 (1978); **68**, 3891 (1978).

[24]The accurate determination of multiple complex resonant frequencies from a spectrum derived from a correlation function has already been demonstrated. See, for example, M. D. Feit and J. A. Fleck, Jr., Appl. Opt. **20**, 2843 (1981).

[25]H. A. Bethe and E. E. Salpeter, *Quantum Mechanics of One and Two-Electron Atoms* (Plenum, New York, 1977), p. 262.

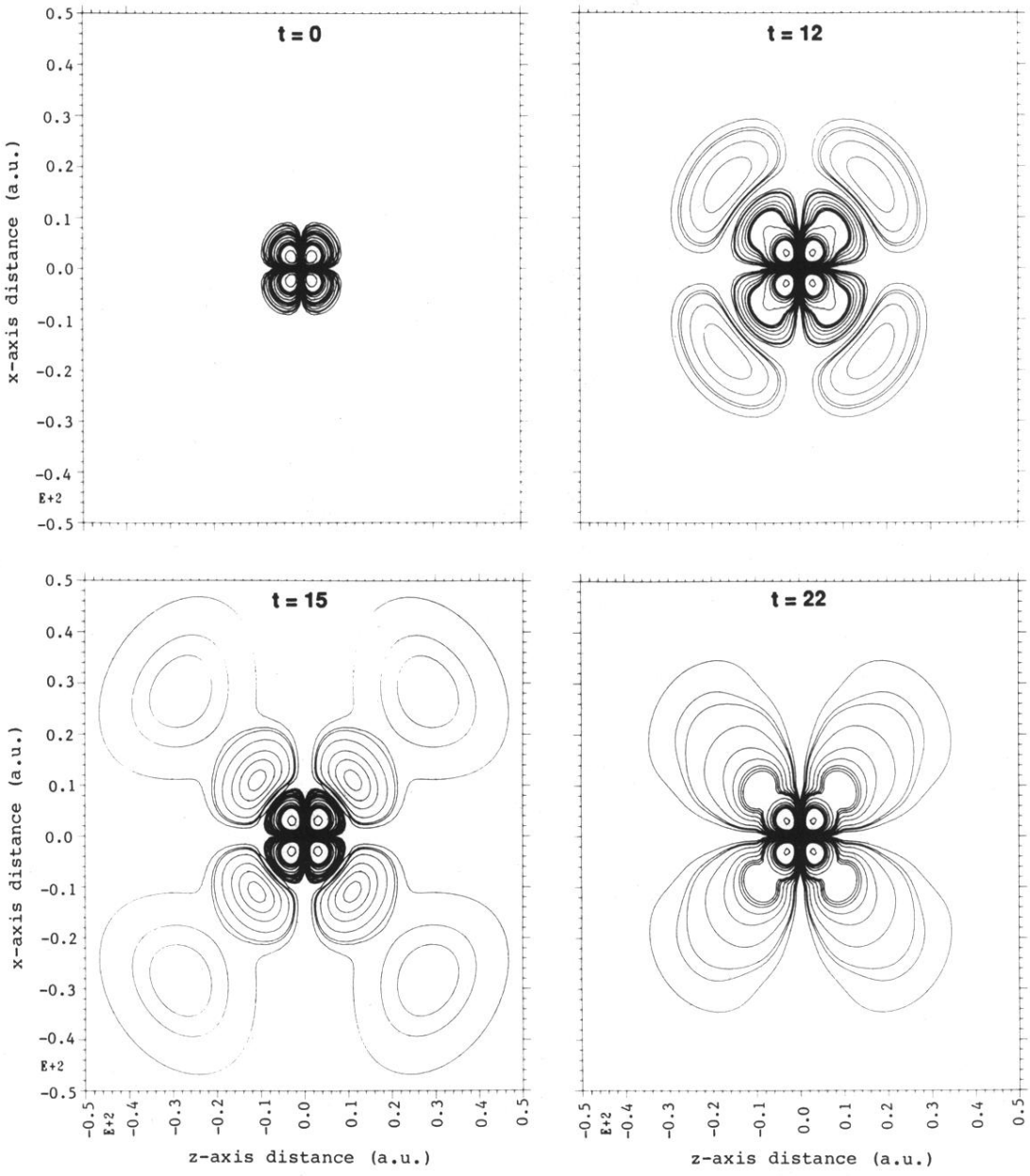

FIG. 5. Contours of equal probability calculated from the wave packet used to generate the spectra in Figs. 3 and 4. Times are indicated in units of 2000 a.u.